From a Collapse-Prone, Insulating Ni-MOF-74 Analog to Crystalline, Porous, and Electrically Conducting PEDOT@MOF Composites

Shiyu Zhang,[†] Weikang Zhang,[†] Ashok Yadav,[†] Jacob Baker,[†] and Sourav Saha*[,†]

[†]Department of Chemistry, Clemson University, Clemson, South Carolina 29634, United States.
*Email: souravs@clemson.edu

Abstract

Electrically conductive, porous MOFs show great promise to help advance electronics and clean energy technologies. However, large porosity usually hinders long-range charge transport, an essential criterion of electrical conductivity, underscoring the need for new strategies to combine these two opposing features and to realize their diverse potentials. All previous strategies to boost the conductivity of porous MOFs by introducing redox-complementary guest molecules, conducting polymers (CP), and metal nanoparticles have led to significant loss of frameworks' porosity and surface areas, which could be otherwise exploited to capture additional guests in electrocatalysis and chemiresistive sensing applications. Herein, we demonstrate for the first time that *in-situ* oxidative polymerization of preloaded 3,4-ethylenedioxythiophene (EDOT) monomers into polyethylenedioxythiophene (PEDOT) polymer inside the hexagonal cavities of an intrinsically insulating Ni_2(NDISA) MOF-74 analog (NDISA = naphthalenediimide *N,N*-disalicylate), which easily collapses and becomes amorphous upon drying, simultaneously enhanced the crystallinity, porosity, and electrical conductivity of the resulting PEDOT@Ni_2(NDISA) composites. At lower PEDOT loading (~22 wt%), not only did the Brunauer-Emmett-Teller surface area of PEDOT@Ni_2(NDISA) composite (926 m^2/g) more than double from that of evacuated pristine Ni_2(NDISA) (387 m^2/g), but also its electrical conductivity (1.1×10^{-5} S/cm) soared 10^5 times from that of the pristine MOF, demonstrating unprecedented dual benefits of our strategy. At higher PEDOT loading (≥33 wt%), the electrical conductivity of Ni_2(NDISA)⊃PEDOT composites further increased modestly (10^{-4} S/cm), but their porosity dropped precipitously, as large amounts of PEDOT filled up the hexagonal MOF channels. Thus, our work presents a simple new strategy to simultaneously boost the structural stability, porosity, and electrical conductivity of intrinsically insulating and collapse-prone MOFs by introducing small amounts of conducting polymers that can not only reinforce the MOF scaffolds and prevent them from collapsing, but also help create a much coveted non-native property by providing charge carriers and charge transport pathways.

Introduction

Semiconducting metal–organic frameworks (MOFs)[1–7] with permanent porosity, ultralow density, and tunable electrical conductivity are in high demand due to their diverse potentials to serve as active components of myriad electronics and clean energy production, transport, and storage devices, such as rechargeable batteries,[8–16] supercapacitors,[17–25] transistors,[26,27] chemiresistive sensors,[28–35] and electrocatalysts.[36–42] Despite remarkable recent advances, generating high intrinsic electrical conductivity in 3D porous MOFs and covalent-organic frameworks (COFs) remains a challenging task chiefly because they often lack efficient well-defined through-bond and/or through-space charge transport pathways.[1,3,43–48] One way to boost the electrical conductivity of highly porous MOFs is to introduce appropriate guest molecules, such as node-coordinating conjugated π-systems, which can bridge coordinatively unsaturated

nodes and thereby promote through-bond charge transport,[49] or redox-complementary π-intercalators that can form extended π-donor/acceptor stacks with the preorganized ligands and thus facilitate through-space charge transport.[50–59] Another strategy to facilitate charge transport across porous MOFs entails *in-situ* polymerization of preloaded monomers into conducting polymers (CPs), such as polyaniline, polypyrrole, polythiophene, and polyethylenedioxythiophene (PEDOT), inside MOF pores,[60–68] or *in-situ* reduction of entrapped metal ions into metal nanoparticles.[69] All existing guest-induced conductivity enhancement strategies, however, boost the frameworks' conductivity at the expense of their porosity and surface areas because the encapsulated guests fill up their cavities.[60–64,69] Even the biporous MOFs having two distinct sets of cavities, such as MIL-101(Cr and Fe) and UiO-66, where the *in-situ* generated CPs selectively occupied the larger pores, suffered 30–70% loss of the original surface areas.[62,63] Therefore, needed is a nifty new strategy that can efficiently boost the frameworks' conductivity while also preserving or even boosting their porosity and surface areas that can be utilized for additional guest binding in potential chemiresistive sensing and electrocatalysis applications.

Recently, Uemura[70] and Queen[71,72] have demonstrated that *in-situ* polymerization of preloaded styrene and dopamine monomers into polystyrene and polydopamine inside collapse-prone Co-pillared paddlewheel MOF and MOF-74 architectures enhanced the structural stability as well as specific surface areas of resulting polymer@MOF composites, as small numbers of polymer chains confined to MOF pores prevented framework collapse upon solvent loss. However, to our knowledge, *in-situ* generated conducting polymers have not yet simultaneously enhanced the structural stability, porosity, and electrical conductivity of resulting CP@MOF composites, which prompted us to realize these unique possibilities.

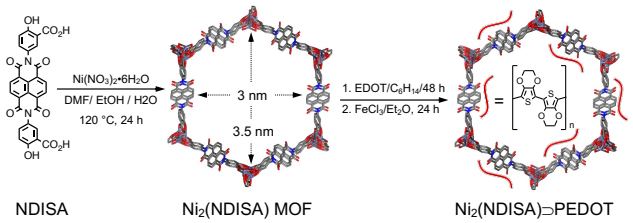

Figure 1. A graphical representation of structural reinforcement and conductivity enhancement of collapse-prone insulating MOFs by in-situ polymerization of conducting polymers.

Herein, we demonstrate that oxidative polymerization of electron-rich ethylenedioxythiophene (EDOT) monomers into PEDOT polymer inside uniform hexagonal channels of an intrinsically insulating, collapse-prone MOF-74 analog, Ni_2(NDISA) (NDIDSA = *N,N*-disalicylate (NDISA)),[73] yielded structurally robust, permanently porous, and semiconducting Ni_2(NDISA)⊃PEDOT nanocomposites (Figure 1). In contrast to intrinsically insulating Ni_2(NDISA), which became amorphous and possessed a modest Brunauer-Emmett-Teller surface area (S_{BET} = 387 m^2/g) after thorough evacuation at 150 °C, the Ni_2(NDISA)⊃PEDOT composites containing different amounts of trapped PEDOT (~22–37 wt%) remained crystalline upon similar activation. More importantly, the Ni_2(NDISA)⊃PEDOT-10 composite containing a smaller amount of trapped PEDOT (~22 wt%) displayed 2.4 times larger surface area (S_{BET} = 926 m^2/g) and 10^5 times higher electrical conductivity (1.1×10^{-5} S/cm) than the pristine MOF. The conductivity of Ni_2(NDISA)⊃PEDOT composites containing larger amounts of PEDOT increased further (~10^{-4} S/cm) but the porosity decreased gradually, as more PEDOT chains filled up the MOF pores. Our studies present a rare, if not the first, example of simultaneous enhancement of structural stability, porosity,

and electrical conductivity of an inherently collapse-prone and insulating MOF by loading it with a small amount of conducting polymer far below the framework's maximum loading capacity.

Results and Discussion

To demonstrate the concept of simultaneous enhancement of structural stability, porosity, and electrical conductivity of inherently collapse-prone and insulating MOFs via *in-situ* polymerization of a conducting polymer, we have employed a MOF-74 analog Ni_2(NDISA), which has large uniform hexagonal channels (pore diameter >3 nm) and a theoretical surface area of 2872 m^2/g,[71] but in practice displays a much smaller S_{BET} (1722 m^2/g) after activation even under supercritical CO_2 condition.[73] Ni_2(NDISA) MOF was synthesized according to a literature protocol[71,73] by heating a solution mixture (DMF/EtOH/H_2O) of NDISA ligand and $Ni(NO_3)_2 \cdot 6H_2O$ (5 equiv.) at 120 °C for 24 h, and subsequently washed with DMF, MeOH, Et_2O, and hexanes (see Supporting Information (SI) for details).

The powder X-ray diffraction (PXRD) pattern of pristine Ni_2(NDISA) MOF containing solvent molecules was fully consistent with its simulated PXRD profile, confirming its periodic structure and phase purity. However, after exchanging DMF with more volatile solvents, such as MeOH, Et_2O, and hexanes, and drying it under vacuum at 150 °C, the resulting material lost crystallinity (Figure 2a) due to partial framework collapse. This observation was consistent with literature reports[71,73] showing other M_2(NDISA) MOF structures also collapsed upon traditional activation. After soaking activated Ni_2(NDISA) MOF in different solvents (DMF, MeOH, hexane, etc.), it failed to regain crystallinity (no PXRD peak), indicating that the framework collapse upon solvent loss was irreversible. However, when stored soaked in different solvents (DMF, MeOH, Et_2O, and hexane) without completely drying, pristine Ni_2(NDISA) MOF remained crystalline and displayed the characteristic PXRD pattern. The N_2-sorption isotherm (Figure 2b) of pristine Ni_2(NDISA) activated under vacuum at 150 °C had a modest S_{BET} of only 387 m^2/g, which is similar to the reported value (433 m^2/g),[71] but far below the theoretical prediction, demonstrating that framework collapse also led to a significant loss of porosity.

Ni_2(NDISA)⊃PEDOT composites containing different amounts (wt%) of encapsulated PEDOT were synthesized as follows: First, Ni_2(NDISA) MOF was loaded with EDOT by soaking it (45 mg) in different concentrations of EDOT/hexane solutions (10, 15, 20, or 30 μL of EDOT in 3 mL hexane) at room temperature for 48 h. The concentrations of EDOT solutions in which a fixed amount of Ni_2(NDISA) was suspended controlled the monomer population inside the MOF, which subsequently dictated the amount (wt%) of PEDOT chains present in the resulting composites. After decanting the solutions of free EDOT, saturated anhydrous $FeCl_3/Et_2O$ solution (5 mL) was added to EDOT-loaded Ni_2(NDISA), and the resulting mixtures were stirred at room temperature for 24 h to allow oxidative polymerization of preloaded EDOT monomers into PEDOT chains. Finally, the materials were washed thoroughly with MeOH and Et_2O until the washing solutions became completely colorless, indicating that the unreacted monomers and oxidizing agent were mostly removed. The resulting dark brownish-black powders were dried under vacuum to obtain Ni_2(NDISA)⊃PEDOT-X (X = 10, 15, 20, and 30) composites containing increasing amounts of trapped PEDOT, which were obtained from 10, 15, 20, and 30 μL of EDOT in hexane (3 mL) solutions, respectively.

Unlike pristine Ni_2(NDISA) MOF, which lost the crystallinity after activation under vacuum at 150 °C, the Ni_2(NDISA)⊃PEDOT-X (X = 10, 15, 20, and 30) composites activated under the same conditions

displayed the characteristic PXRD signals (Figure 2a) of as-synthesized Ni_2(NDISA), indicating that *in-situ* generated PEDOT chains located inside the pores helped reinforce the crystalline MOF structure and prevented it from collapsing upon solvent loss. While all four N_2(NDISA)⊃PEDOT-X (X = 10, 15, 20, and 30) composites displayed the characteristic PXRD peaks of the MOF, the peak intensities decreased with the increasing amounts of amorphous PEDOT polymers present in the composites.

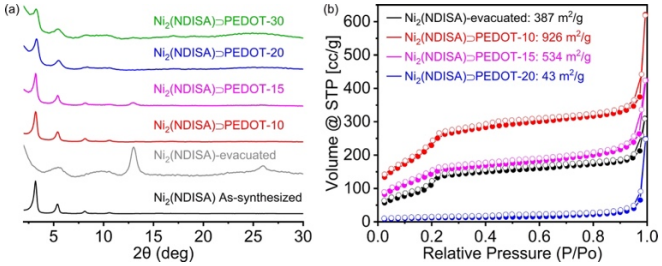

Figure 2. (a) The PXRD profiles of pristine Ni_2(NDISA) and Ni_2(NDISA)⊃PEDOT-X (X = 10, 15, 20, and 30) composites containing different amounts of PEDOT. (b) The N_2 sorption isotherms (77 K) of Ni_2(NDISA) and Ni_2(NDISA)⊃PEDOT-X composites (solid circles: adsorption, open circles: desorption).

The amounts of *in-situ* generated PEDOT trapped inside Ni_2(NDISA) were determined by two separate methods— elemental and analyses gravimetric (Table S1)—which were in good agreement. The precise amount of PEDOT present in each composite was determined from the N to S ratios, the signature elements of NDISA ligand of the MOF and embedded PEDOT, respectively, measured by elemental analysis. The observed S:N ratios in Ni_2(NDISA)⊃PEDOT-X composites (X = 10, 15, 20, and 30) were 4.5 to 2.8 (1.6), 5.5 to 2.8 (2.0), 6.9 to 2.5 (2.8), and 8.3 to 2.5 (3.4), respectively, which corresponded to ca. 22, 26, 33, and 37 wt% of PEDOT, respectively (see SI for detailed calculations). Furthermore, based on the weight of in-situ generated PEDOT extracted from a known quantity of each composite (by digesting the MOF scaffold with aqueous NH_4OH solution, see SI for details), Ni_2(NDISA)⊃PEDOT-X (X = 10, 15, 20, and 30) composites contained ca. 22, 29, 36, and 39 wt% of PEDOT, respectively. These results confirmed that the PEDOT contents in Ni_2(NDISA)⊃PEDOT-X composites increased systematically with increasing EDOT concentrations used for monomer loading prior to *in-situ* oxidative polymerization.

Nitrogen sorption analysis performed at 77 K (Figure 2b) revealed that whereas Ni_2(NDISA) MOF evacuated at 150 °C has a modest S_{BET} of 387 m^2/g, similarly activated Ni_2(NDISA)⊃PEDOT-10 has 2.4 times larger S_{BET} (926 m^2/g), suggesting that a relatively small amount of PEDOT (22 wt%) trapped inside the MOF pores helped stabilize its crystalline structure and prevented it from collapsing upon solvent loss. As the PEDOT content (wt%) increased, S_{BET} of the composites decreased gradually establishing a clear trend—i.e., 534 m^2/g for Ni_2(NDISA)⊃PEDOT-15 and 43 m^2/g for Ni_2(NDISA)⊃PEDOT-20—as the higher PEDOT contents filled up the MOF pores.

The presence of PEDOT in Ni_2(NDISA)⊃PEDOT-X composites was further verified by FT-IR and scanning electron microscopy coupled with energy dispersive X-ray (SEM-EDX) analyses. The FT-IR spectra (Figure S1) of the composites, as well as the extracted PEDOT, revealed characteristic C–S stretching signals at 670, 830, 906, and 976 cm^{-1}.[62,74] The SEM images of pristine Ni_2(NDISA) MOF and representative Ni_2(NDISA)⊃PEDOT-10 composite (Figure 3) showed rectangular rod-shaped crystals, indicating that MOF crystallites remained largely intact upon *in-situ* oxidative polymerization of PEDOT.

Furthermore, SEM-EDX analysis of Ni_2(NDISA)⊃PEDOT-10 revealed the coexistence of the signature elements of Ni_2(NDISA) (Ni and N) and PEDOT (S).

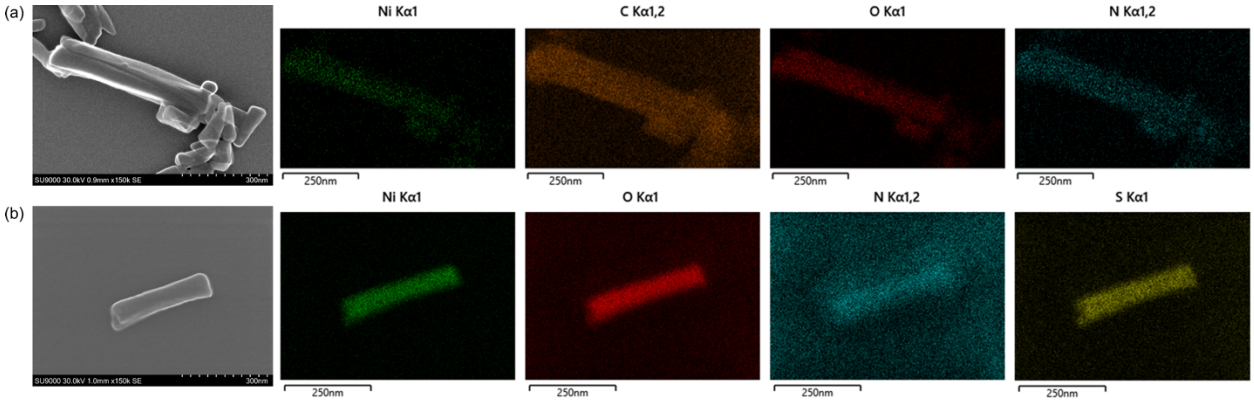

Figure 3. SEM and SEM-EDX images of (a) pristine Ni_2(NDISA) and (b) a representative Ni_2(NDISA)⊃PEDOT-10 composite show the rod-shaped MOF crystals and the coexistence of signature elements (Ni, N, and S) of both components in the latter.

Thermogravimetric analysis (TGA, Figure S2) showed that pristine Ni_2(NDISA) MOF underwent significant weight loss (ca. 17%) until 150 °C due to solvent loss, whereas the Ni_2(NDISA)⊃PEDOT-X composites containing ca. 22–37 wt% PEDOT underwent much smaller weight loss (ca. 10%) up to this point. The pristine MOF as well as Ni_2(NDISA)⊃PEDOT-X composites decomposed at ca. 300 °C. In contrast, bulk PEDOT generated in the absence of the MOF showed negligible weight loss (≤ 2%) before decomposing at ~250 °C. The residual weights of thermally decomposed Ni_2(NDISA)⊃PEDOT-X composites, which primarily stemmed from the Ni-nodes of the MOF, decreased with increasing PEDOT content, as the organic components, i.e., NDISA ligand and PEDOT, mostly disappeared as volatile gasses upon pyrolysis.

The UV-Vis-NIR diffuse-reflectance spectrum (DRS) (Figure 4a) of orange-colored pristine Ni_2(NDISA) MOF showed a peak at ca. 410 nm, but no notable peak at longer wavelengths, whereas bulk PEDOT prepared under the same oxidative polymerization conditions (see SI) without the MOF displayed a broad signal (500–1200 nm) centered on ca. 700 nm. The DRS plots of Ni_2(NDISA)⊃PEDOT-X composites featured the characteristic signals of both MOF and PEDOT, confirming their coexistence. The shifting of the MOF and PEDOT peaks in the composites could be attributed to intermolecular interactions. The corresponding Tauc plots (Figure 4b) revealed the optical band gaps (E_{op}) of pristine MOF (3.10 eV), bulk PEDOT (1.48 eV), Ni_2(NDISA)⊃PEDOT-10 (1.84 eV), Ni_2(NDISA)⊃PEDOT-20 (1.79 eV), and Ni_2(NDISA)⊃PEDOT-30 (1.76 eV), indicating that E_{op} of the composites narrowed slightly with increasing PEDOT content.

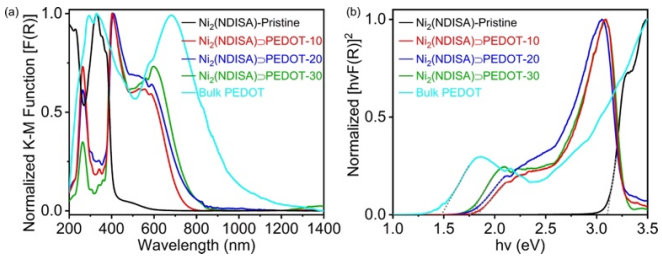

Figure 4. (a) UV-Vis-NIR DRS and (b) Tauc plots of pristine Ni_2(NDISA), PEDOT, and Ni_2(NDISA)⊃PEDOT-X composites.

Finally, the electrical conductivities of pristine Ni_2(NDISA), Ni_2(NDISA)⊃PEDOT-X composites containing different amounts of PEDOT, *in-situ* generated PEDOT extracted from the composites, and bulk PEDOT formed in the absence of the MOF were determined from their respective current–voltage (*I-V*) plots (Figure 5a) measured by two-probe method using pressed pellets of each material placed between two stainless steel electrodes encased inside a snugly fit Teflon tube. Whereas pristine Ni_2(NDISA) MOF displayed negligible electrical conductivity (3.4×10^{-10} S/cm), the Ni_2(NDISA)⊃PEDOT-X composites (X = 10, 15, 20, and 30) displayed up to 10^6 times higher conductivity, which increased with the increasing PEDOT content as follows: 1.1×10^{-5}, 4.3×10^{-5}, 1.2×10^{-4}, and 2.3×10^{-4} S/cm, respectively. Thus, Ni_2(NDISA)⊃PEDOT-10 composite containing the lowest amount of trapped PEDOT (22 wt%) attained 10^5 times higher electrical conductivity as well as 2.4 times higher S_{BET} than the pristine MOF, as small number of PEDOT chains not only facilitated charge transport but also reinforced the MOF scaffold without blocking the pores. As the amount of PEDOT chains (≥33 wt%) trapped inside the MOF increased, the electrical conductivity of the composites increased by another order of magnitude (to 10^{-4} S/cm), but the surface area decreased significantly, as the large number of PEDOT chains blocked the MOF pores (Table 1). In contrast, in all previous cases,[60–68] the *in-situ* generated CPs trapped inside the MOF pores enhanced the frameworks' electrical conductivity only at the expense of their porosity. Even biporous MIL-101(Cr and Fe) and UiO-66 having two different sized and shaped pores, which hosted CPs inside the larger hexagonal pores while the smaller trigonal ones remained mostly vacant, lost substantial (30–70%) surface area after in-situ polymerization.

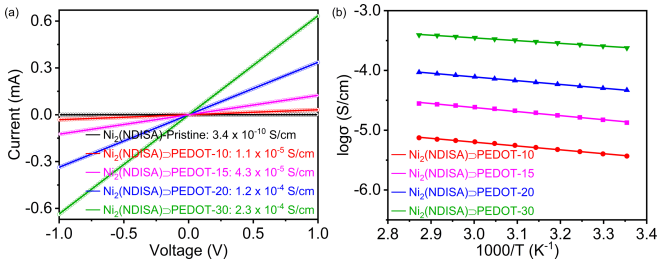

Figure 5. (a) The *I–V* plots and (b) Arrhenius plots of pristine Ni_2(NDISA) and Ni_2(NDISA)⊃PEDOT-X (X = 10, 15, 20, and 30) composites reveal the electrical conductivities and activation energies, respectively.

In a control experiment, a blend of Ni_2(NDISA) and separately prepared PEDOT (78:22 w/w ratio, comparable to PEDOT content in Ni_2(NDISA)⊃PEDOT-10) displayed much lower conductivity ($2.1 \times 10^{-}$

^{8} S/cm) than the composites containing *in-situ* generated PEDOT, suggesting that PEDOT chains located inside the MOF pores facilitated long-range charge transport and helped improve the conductivity of the composites. Furthermore, the *in-situ* generated PEDOT extracted from each of these composites by digesting the MOF also displayed (Figure S3) displayed slightly higher electrical conductivity (1.1–1.5 × 10^{-4} S/cm) than bulk PEDOT (6.4 × 10^{-5} S/cm) prepared under the same conditions but without the MOF, showing another benefit of Ni_2(NDISA)⊃PEDOT composites.

Table 1. The relationships between PEDOT content (wt%), S_{BET}, and electrical conductivity (σ) of Ni_2(NDISA)⊃PEDOT composites.

Materials	PEDOT wt%[a]	S_{BET} (m^2/g)[b]	σ (S/cm)[c]
Evacuated Ni_2(NDISA)	0	387	3.4×10^{-10}
Ni_2(NDISA)⊃PEDOT-10	22	926	1.1×10^{-5}
Ni_2(NDISA)⊃PEDOT-15	26	534	4.3×10^{-5}
Ni_2(NDISA)⊃PEDOT-20	33	43	1.2×10^{-4}
Ni_2(NDISA)⊃PEDOT-30	37	–	2.3×10^{-4}

[a]based on elemental analysis (Table S1), [b]experimental values, [c]at 298 K.

Temperature-dependent conductivity measurements (Figure S4) revealed thermally activated charge transport in Ni_2(NDISA)⊃PEDOT-X composites, which is a typical semiconductor behavior. From the Arrhenius plots of temperature-dependent conductivity data (Figure 5b), the thermal activation energies of Ni_2(NDISA)⊃PEDOT-X composites (X = 10, 15, 20, and 30) were estimated to be 130, 126, 120, and 100 meV, respectively, which decreased gradually with increasing PEDOT population.

Conclusions

In summary, herein, we have demonstrated for the first time that *in-situ* oxidative polymerization of PEDOT inside the hexagonal pores of an easily collapsible and electrically insulating MOF-74 analog simultaneously enhanced the structural robustness, crystallinity, internal surface area, and electrical conductivity of resulting Ni_2(NDISA)⊃PEDOT composites (Table 1). Evacuated Ni_2(NDISA)⊃PEDOT-10 composite containing a smaller amount of PEDOT (22 wt%) displayed 2.4 times larger surface area and 10^5 times higher electrical conductivity than evacuated pristine Ni_2(NDISA), as the small number of trapped PEDOT chains simultaneously reinforced the MOF scaffold, preventing it from collapsing upon solvent loss and provided long-range conduction pathways. At higher PEDOT content, the electrical conductivity of Ni_2(NDISA)⊃PEDOT composites further increased slightly, but their surface areas dropped significantly, as greater number of PEDOT chains filled up the hexagonal MOF-74 pores. In principle, this strategy could be implemented to convert other collapse-prone insulating frameworks into robust, permanently porous, end electrically conductive MOF–polymer composites via in-situ formation of conducting polymers at much below the framework's maximum loading capacity.

■ ASSOCIATED CONTENT

Supporting Information

Supporting Information is available free of charge at https://.... Experimental details and additional data (PDF).

■ AUTHOR INFORMATION

Corresponding Author

Sourav Saha — Department of Chemistry, Clemson University, Clemson, South Carolina 29634, United States; orcid.org/0000-0001-6610-4820; Email: souravs@clemson.edu

Authors

Shiyu Zhang — Department of Chemistry, Clemson University, Clemson, South Carolina 29634, United States. Orcid.org/0009-0008-5615-4654

Weikang Zhang — Department of Chemistry, Clemson University, Clemson, South Carolina 29634, United States; orcid.org/0009-0008-5454-5061

Ashok Yadav — Department of Chemistry, Clemson University, Clemson, South Carolina 29634, United States; orcid.org/0000-0002-9414-2450

Jacob Baker — Department of Chemistry, Clemson University, Clemson, South Carolina 29634, United States.

Author Contributions

The manuscript was written through contributions of all authors. All authors approved the final version of the manuscript.

Notes

The authors declare no competing financial interest.

■ ACKNOWLEDGEMENTS

This work was supported by the National Science Foundation (award nos. DMR-1809092 and DMR-2321365). JB acknowledges the support from NSF REU award no. CHE-2050042.

■ REFERENCES

(1) Xie, L. S.; Skorupskii, G.; Dincă, M. Electrically Conductive Metal–Organic Frameworks. *Chem. Rev.* **2020**, *120*, 8536–8580.

(2) Leong, C. F.; Usov, P. M.; D'Alessandro, D. M. Intrinsically Conducting Metal-Organic Frameworks. *MRS Bull.* **2016**, *41*, 858–864.

(3) Sun, L.; Campbell, M. G.; Dincă, M. Electrically Conductive Porous Metal–Organic Frameworks. *Angew. Chem. Int. Ed.* **2016**, *55*, 3566–3579.

(4) Jacoby, M. Conductive MOFs: Surprising Charge Transport Property Could Lead to New Applications. *C&EN* **2021**, *99* (43), 30–34.

(5) Johnson, E.; Ilic, S.; Morris, A. J. Design Strategies for Enhanced Conductivity in Metal-Organic Frameworks. *ACS Cent. Sci*. **2021**, *7*, 445–453.

(6) Ko, M.; Mendecki, L.; Mirica, K. A. Conductive Two-Dimensional Metal−Organic Frameworks as Multifunctional Materials. *Chem. Commun*. **2018**, *54*, 7873−7891.

(7) Hendon, C. H.; Tiana, A.; Walsh, A. Conductive Metal–Organic Frameworks and Networks: Fact or Fantasy? *Phys. Chem. Chem. Phys.* **2012**, *14*, 13120–13132.

(8) Wen, X.; Zhang, Q.; Guan, J. Applications of Metal–Organic Framework-Derived Materials in Fuel Cells and Metal-Air Batteries. *Coord. Chem. Rev*. **2020**, *409*, 213214.

(9) Jiang, H.; Liu, X.-C.; Wu, Y.; Shu, Y.; Gong, X.; Ke, F.-S.; Deng, H. Metal-Organic Frameworks for High Charge-Discharge Rates in Lithium-Sulfur Batteries. *Angew. Chem. Int. Ed*. **2018**, *57*, 3916−3921.

(10) Zhang, Z.; Awaga, K.; Redox-Active Metal-Organic Frameworks as Electrode Materials for Batteries. *MRS Bull.* **2016**, 41, 883–889.

(11) Panda, D. K.; Maity, K.; Palukoshka, A.; Ibrahim, F.; Saha, S. Li^+ Ion Conducting Sulfonate-Based Neutral Metal–Organic Framework. *ACS Sus. Chem. Eng.* **2019**, *7*, 4619–4624.

(12) Nam, K. W.; Park, S. S.; dos Reis, R.; Dravid, V. P.; Kim, H.; Mirkin, C. A.; Stoddart, J. F. Conductive 2D Metal-Organic Framework for High-Performance Cathodes in Aqueous Rechargeable Zinc Batteries. *Nat. Commun*. **2019**, *10*, 4948.

(13) Morozan, A.; Jaouen, F. Metal Organic Frameworks for Electrochemical Applications. *Energy Environ. Sci.* **2012,** *5*, 9269–9290. 8-12

(14) Lim, D.-W.; Kitagawa, H. Proton Transport in Metal–Organic Frameworks. *Chem. Rev*. **2020**, *120*, 8416–8567.

(15) Park, S. S.; Tulchinsky, Y.; Dincă, M. Single-ion Li^+, Na^+, and Mg^{2+} Solid Electrolytes Supported by a Mesoporous Anionic Cu–Azolate Metal–Organic Framework. *J. Am. Chem. Soc.* **2017,** *139*, 13260–13263.

(16) Shinde, S. S.; Lee, C. H.; Jung, J.-Y.; Wagh, N. K.; Kim, S.-H.; Kim, D.-H.; Lin, C.; Lee, S. U.; Lee, J.-H. Unveiling Dual-Linkage 3D Hexaiminobenzene Metal-Organic Frameworks towards Long-Lasting Advanced Reversible Zn-Air Batteries. *Energy Environ. Sci*. **2019**, *12*, 727−738.

(17) Sheberla, D.; Bachman, J. C.; Elias, J. S.; Sun, C.-J.; Shao-Horn, Y.; Dincă, M. Conductive MOF Electrodes for Stable Supercapacitors with High Areal Capacitance. *Nat. Mater.* **2017**, *16*, 220−224.

(18) Xu, G.; Nie, P.; Dou, H.; Ding, B.; Li, L.; Zhang, X. Exploring Metal Organic Frameworks for Energy Storage in Batteries and Supercapacitors. *Mater. Today* **2017**, 20, 191–209.

(19) Li, W.-H.; Ding, K.; Tian, H.-R.; Yao, M.-S.; Nath, B.; Deng, W.-H.; Wang, Y.; Xu, G. Conductive Metal-Organic Framework Nanowire Array Electrodes for High-Performance Solid-State Supercapacitors. *Adv. Funct.* Mater. **2017**, *27*, 1702067.

(20) Wang, L.; Han, Y. Z.; Feng, X.; Zhou, J. W.; Qi, P. F.; Wang, B., Metal-Organic Frameworks for Energy Storage: Batteries and Supercapacitors. *Coord. Chem. Rev.* **2016,** *307*, 361–381.

(21) Xia, W.; Mahmood, A.; Zou, R. Q.; Xu, Q. Metal-Organic Frameworks and Their Derived Nanostructures for Electrochemical Energy Storage and Conversion. *Energy Environ. Sci.* **2015,** *8*, 1837–1866.

(22) Ke, F. S.; Wu, Y. S.; Deng, H. X., Metal-Organic Frameworks for Lithium Ion Batteries and Supercapacitors. *J. Solid State Chem.* **2015,** *223*, 109–121.

(23) Wang, H.; Zhu, Q.-L.; Zou, R.; Xu, Q. Metal-Organic Frameworks for Energy Applications. *Chem* **2017**, *2*, 52−80.

(24) Wu, H. B.; Lou, X. W. Metal-Organic Frameworks and Their Derived Materials for Electrochemical Energy Storage and Conversion: Promises and Challenges. *Sci. Adv.* **2017**, *3*(12):eaap9252.

(25) Wu, H.; Zhang, W.; Kandambeth, S.; Shekhah, O.; Eddaoudi, M.; Alshareef, H. N. Conductive Metal-Organic Frameworks Selectively Grown on Laser-Scribed Graphene for Electrochemical Microsupercapacitors. *Adv. Energy Mater*. **2019**, *9*, 1900482.

(26) Wu, G.; Huang, J.; Zang, Y.; He, J.; Xu, G. Porous Field-Effect Transistors Based on a Semiconductive Metal−Organic Framework. *J. Am. Chem. Soc*. **2017**, *139*, 1360−1363.

(27) Wang, B.; Luo, Y.; Liu, B.; Duan, G. Field-Effect Transistor Based on an in Situ Grown Metal−Organic Framework Film as a Liquid-Gated Sensing Device. *ACS Appl. Mater. Interfaces* **2019**, *11*, 35935−35940.

(28) Stassen, I.; Burtch, N.; Talin, A.; Falcaro, P.; Allendorf, M.; Ameloot, R. An Updated Roadmap for the Integration of Metal–Organic Frameworks with Electronic Devices and Chemical Sensors. *Chem. Soc. Rev.* **2017**, *46*, 3185–3241.

(29) Campbell, M. G.; Liu, S. F.; Swager, T. M.; Dincă, M. Chemiresistive Sensor Arrays from Conductive 2D Metal-Organic Frameworks. *J. Am. Chem. Soc.* **2015**, *137*, 13780−13783.

(30) Campbell, M. G.; Sheberla, D.; Liu, S. F.; Swager, T. M.; Dincă, M. Cu_3(Hexaiminotriphenylene)$_2$: An Electrically Conductive 2D Metal-Organic Framework for Chemiresistive Sensing. *Angew. Chem. Int. Ed*. **2015**, *54*, 4349−4352.

(31) Koo, W.-T.; Jang, J.-S.; Kim, I.-D. Metal-Organic Frameworks for Chemiresistive Sensors. *Chem* **2019**, *5*, 1938−1963.

(32) Aubrey, M. L.; Kapelewski, M. T.; Melville, J. F.; Oktawiec, J.; Presti, D.; Gagliardi, L.; Long, J. R. Chemiresistive Detection of Gaseous Hydrocarbons and Interrogation of Charge Transport in Cu[Ni(2,3-Pyrazinedithiolate)$_2$] by Gas Adsorption. *J. Am. Chem. Soc.* **2019**, *141*, 5005−5013.

(33) Yao, M.-S.; Lv, X.-J.; Fu, Z.-H.; Li, W.-H.; Deng, W.-H.; Wu, G.-D.; Xu, G. Layer-by-Layer Assembled Conductive Metal-Organic Framework Nanofilms for Room-Temperature Chemiresistive Sensing. *Angew. Chem. Int. Ed*. **2017**, *56*, 16510−16514.

(34) Yao, M.-S.; Zheng, J.-J.; Wu, A.-Q.; Xu, G.; Nagarkar, S. S.; Zhang, G.; Tsujimoto, M.; Sakaki, S.; Horike, S.; Otake, K.; Kitagawa, S. A Dual-Ligand Porous Coordination Polymer Chemiresistor with Modulated Conductivity and Porosity. *Angew. Chem. Int. Ed*. **2020**, *59*, 172−176.

(35) Rubio-Gimenez, V.; Almora-Barrios, N.; Escorcia-Ariza, G.; Galbiati, M.; Sessolo, M.; Tatay, S.; Marti-Gastaldo, C. Origin of the Chemiresistive Response of Ultrathin Films of Conductive Metal-Organic Frameworks. *Angew. Chem. Int. Ed*. **2018**, *57*, 15086−15090.

(36) Downes, C. A.; Marinescu, S. C. Electrocatalytic Metal−Organic Frameworks for Energy Applications. *ChemSusChem* **2017**, *10*, 4374−4392.

(37) Miner, E. M.; Wang, L.; Dincă, M. Modular O_2 Electroreduction Activity in Triphenylene-Based Metal-Organic Frameworks. *Chem. Sci*. **2018**, *9*, 6286−6291.

(38) Miner, E. M.; Fukushima, T.; Sheberla, D.; Sun, L.; Surendranath, Y.; Dincă, M. Electrochemical Oxygen Reduction Catalysed by Ni_3(Hexaiminotriphenylene)$_2$. *Nat. Commun*. **2016**, *7*, 10942.

(39) Lin, S.; Pineda-Galvan, Y.; Maza, W. A.; Epley, C. C.; Zhu, J.; Kessinger, M. C.; Pushkar, Y.; Morris, A. J. Electrochemical Water Oxidation by a Catalyst-Modified Metal–Organic Framework Thin Film. *ChemSusChem* **2017**, 10, 514–522.

(40) Li, S. L.; Xu, Q. Metal-Organic Frameworks as Platforms for Clean Energy. *Energy Environ. Sci.* **2013,** *6*, 1656–1683.

(41) Clough, A. J.; Yoo, J. W.; Mecklenburg, M. H.; Marinescu, S. C. Two-Dimensional Metal−Organic Surfaces for Efficient Hydrogen Evolution from Water. *J. Am. Chem. Soc*. **2015**, *137*, 118−121.

(42) Downes, C. A.; Clough, A. J.; Chen, K.; Yoo, J. W.; Marinescu, S. C. Evaluation of the H_2 Evolving Activity of Benzenehexathiolate Coordination Frameworks and the Effect of Film Thickness on H_2 Production. *ACS Appl. Mater. Interfaces* **2018**, *10*, 1719−1727.

(43) Gordillo, M. A.; Saha, S. Strategies to Improve Electrical and Ionic Conductivities of Metal–Organic Frameworks. *Comments on Inorg. Chem.* **2020**, *40*, 86–106.

(44) Zhang, S.; Panda, D. K.; Yadav. A.; Zhou, W.; Saha, S. Effects of Intervalence Charge Transfer Interaction Between π-Stacked Mixed Valent Tetrathiafulvalene Ligands on the Electrical Conductivity of 3D Metal–Organic Frameworks. *Chem. Sci.* **2021**, *12*, 13379–13391.

(45) Yadav, A.; Panda, D. K.; Zhang, S.; Zhou, W.; Saha, S. Electrically Conductive 3D Metal–Organic Framework Featuring π-Acidic Hexaazatriphenylene Hexacarbonitrile Ligands with Anion–π Interaction and Efficient Charge Transport Capabilities. *ACS Appl. Mater. Interfaces* **2020**, 12, 40613–40619.

(46) Dolgopolova, E. A.; Galitskiy, V. A.; Martin, C. R.; Gregory, H. N.; Yarbrough, B. J.; Rice, A. M.; Berseneva, A. A.; Ejegbavwo, O. A.; Stephenson, K. S.; Kittikhunnatham, P.; Karakalos, S. G.; Smith, M. D.; Greytak, A. B.; Garashchuk, S.; Shustova, N. B. Connecting Wires: Photoinduced Electronic Structure Modulation in Metal−Organic Frameworks. *J. Am. Chem. Soc*. **2019**, *141*, 5350−5358.

(47) Goswami, S.; Hod, I.; Duan, J. D.; Kung, C.-W.; Rimoldi, M.; Malliakas, C. D.; Palmer, R. H.; Farha, O. K.; Hupp, J. T. Anisotropic Redox Conductivity within a Metal−Organic Framework. *J. Am. Chem. Soc*. **2019**, *141*, 17696−17702.

(48) Haldar, S.; Rase, D.; Shekhar, P.; Jain, C.; Vinod, C. P.; Zhang, E.; Shupletsov, L.; Kaskel, S.; Vaidhyanathan, R. Incorporating Conducting Polypyrrole into a Polyimide COF for Carbon-Free Ultra-High Energy Supercapacitor. *Adv. Energy Mater.* **2022**, *12*, 2200754.

(49) Talin, A. A.; Centrone, A.; Ford, A. C.; Foster, M. E.; Stavila, V.; Haney, P.; Kinney, R. A.; Szalai, V.; Gabaly, F. E.; Yoon, H. P.; Léonard, F.; Allendorf, M. D.; Tunable Electrical Conductivity in Metal-Organic Framework Thin-Film Devices. *Science* **2014**, *343*, 66–69.

(50) Kung, C.-W.; Otake, K.; Buru, C. T.; Goswami, S.; Cui, Y.; Hupp, J. T.; Spokoyny, A. M.; Farha, O. K. Increased Electrical Conductivity in a Mesoporous Metal−Organic Framework Featuring Metallacarboranes Guests. *J. Am. Chem. Soc*. **2018**, *140*, 3871−3875.

(51) Guo, Z.; Panda, D. K.; Maity, K.; Lindsey, D.; Parker, T. G.; Albrecht-Schmitt, T. E.; Barreda-Esparza, J. L.; Xiong, P.; Zhou, W.; Saha, S., Modulating Electrical Conductivity of Metal–Organic Framework Films with Intercalated Guest π-Systems. *J. Mater. Chem. C* **2016**, *4*, 894–899.

(52) Guo, Z.; Panda, D. K.; Gordillo, M. A; Khatun, A.; Wu, H.; Zhou, W.; Saha, S. Lowering Band Gap of an Electroactive Metal–Organic Framework via Complementary Guest Intercalation. *ACS Appl. Mater. Interfaces* **2017**, *9*, 32413–32417.

(53) Yadav, A.; Zhang, S.; Benavides, P. A.; Zhou, W.; Saha, S. Electrically Conductive π-Intercalated Graphitic Metal-Organic Framework Containing Alternate π-Donor/Acceptor Stacks. *Angew. Chem. Int. Ed.* **2023**, e202303819.

(54) Gordillo, M. A.; Benavides, P. A.; Panda, D. K.; Saha, S. Advent of Electrically Conducting Double-Helical Metal–Organic Frameworks Featuring Butterfly-Shaped Electron Rich π-Extended Tetrathiafulvalene Ligands. *ACS Appl. Mater. Interfaces* **2020**, *12*, 12955–12961.

(55) Goswami, S.; Ray, D.; Otake, K.; Kung, C.-W.; Garibay, S. J.; Islamoglu, T.; Atilgan, A.; Cui, Y.; Cramer, C. J.; Farha, O. K.; Hupp, J. T. A Porous, Electrically Conductive Hexa-Zirconium(IV) Metal−Organic Framework. *Chem. Sci*. **2018**, *9*, 4477−4482.

(56) Su, J.; Yuan, S.; Wang, H.-Y.; Huang, L.; Ge, J.-Y.; Joseph, E.; Qin, J.; Cagin, T.; Zuo, J.-L.; Zhou, H.-C. Redox-Switchable Breathing Behavior in Tetrathiafulvalene-Based Metal–Organic Frameworks. *Nat. Commun.* **2017**, *8*, 2008–2016.

(57) Wang, H.-Y.; Ge, J.-Y.; Hua, C.; Jiao, C.-Q.; Wu, Y.; Leong, C. F.; D'Alessandro, D. M.; Liu, T.; Zuo, J.-L. Photo- and Electronically Switchable Spin-Crossover Iron(II) Metal-Organic Frameworks Based on a Tetrathiafulvalene Ligand. *Angew. Chem. Int. Ed.* **2017**, *56*, 5465–5470.

(58) Murase, R.; Leong, C. F.; D'Alessandro, D. M. Mixed Valence as a Strategy for Achieving Charge Delocalization in Semiconducting and Conducting Framework Materials. *Inorg. Chem*. **2017**, *56*, 14373−14382.

(59) Su, J.; Hu, T.-H.; Murase, R.; Wang, H.-Y.; D'Alessandro, D. M.; Kurmoo, M.; Zuo, J.-L. Redox Activities of Metal–Organic Frameworks Incorporating Rare-Earth Metal Chains and Tetrathiafulvalene Linkers. *Inorg. Chem.* **2019**, *58*, 3698–3706.

(60) Khatun, A.; Yadav, A.; Zhang, S.; Saha, S. Transforming an Insulating Metal–Organic Framework into Electrically Conducting Metal–Organic Framework⊃Conducting Polymer Composites. *Mater. Today Chem.* **2022**, 24, 100981.

(61) Salcedo-Abraira, P.; Santiago-Portillo, A.; Atienzar, P.; Bordet, P.; Salles, F.; Guillou, N.; Elkaim, E.; Garcia, H.; Navalon, S. Horcajada, P. A Highly Conductive Nanostructured PEDOT Polymer Confined into the Mesoporous MIL-100(Fe). *Dalton Trans.* **2019**, ***48***, 9807–9817.

(62) Le Ouay, B.; Boudot, M.; Kitao, T.; Yanagida, T.; Kitagawa, S.; Uemura, T. Nanostructuration of PEDOT in Porous Coordination Polymers for Tunable Porosity and Conductivity. *J. Am. Chem. Soc.* **2016**, *138*, 10088−10091.

(63) Jadhav, A.; Gupta, K.; Ninawe, P.; Ballav, N. Imparting Multifunctionality by Utilizing Biporosity in a Zirconium-Based Metal–Organic Framework. *Angew. Chem. Int. Ed.* **2020**, ***132***, 2235–2239.

(64) Wang, Y.; Wang, L.; Huang, W.; Zhang, T.; Hu, X.; Perman, J. A.; Ma, S. Metal-Organic Framework and Conducting Polymer Based Electrochemical Sensor for High Performance Cadmium Ions Detection. *J. Mater. Chem. A* **2017**, *5*, 8385-8393.

(65) Haldar, R.; Sen, B.; Hurrle, S.; Kiato, T.; Sankhla, R.; Kühl, B.; Welle, A.; Heissler, S.; Brenner-Weiss, G.; Thissen, P.; Uemura, T.; Gliemann, H.; Barner-Kowollik, C.; Wöll, C. Oxidative Polymerization of Terthiophene and a Substituted Thiophene Monomer in Metal-Organic Framework Thin Films. *Eur. Polymer J.* **2018**, *109*, 162–168.

(66) MacLean, M. W. A.; Kiato, T.; Suga, T.; Mizuno, M.; Seki, S.; Uemura, T.; Kitagawa, S. Unraveling Inter- and Intrachain Electronics in Polythiophene Assemblies Mediated by Coordination Nanospaces. *Angew. Chem. Int. Ed*. **2016**, *55*, 708−713.

(67) Dhara, B.; Nagarkar, S. S.; Kumar, J.; Kumar, V.; Jha, P. K.; Ghosh, S. K.; Nair, S.; Ballav, N. Increase in Electrical Conductivity of MOF to Billion-Fold upon Filling the Nanochannels with Conducting Polymer. *J. Phys. Chem. Lett.* **2016**, *7*, 2945−2950.

(68) Yang, S.; Karve, V. V.; Justin, A.; Kochetygov, I.; Espín, J.; Asgari, M.; Trukhina, O.; Sun, D. T.; Peng, L.; Queen, W. L. Enhancing MOF Performance Through the Introduction of Polymer Guests. *Coord. Chem. Rev.* **2021**, *427*, 213525.

(69) Gordillo, M. A.; Benavides, P. A.; Ma, K.; Saha, S. Transforming an Insulating Metal–Organic Framework (MOF) into Semiconducting MOF/Gold Nanoparticle (AuNP) and MOF/Polymer/AuNP Composites to Gain Electrical Conductivity. *ACS Appl. Nano Mater*. **2022**, *5*, 13912–13920.

(70) Le Ouay, B.; Kitagawa, S.; Uemura, T. Opening of an Accessible Microporosity in an Otherwise Nonporous Metal–Organic Framework by Polymeric Guests. *J. Am. Chem. Soc.* **2017**, *139*, 7886−7892.

(71) Peng, L.; Yang, S.; Jawahery, S.; Moosavi, S. M.; Huckaba, A. J.; Asgari, M.; Oveisi, E.; Nazeeruddin, M. K.; Smit, B.; Queen, W. L. Preserving Porosity of Mesoporous Metal-Organic Frameworks through the Introduction of Polymer Guests. *J. Am. Chem. Soc.* **2019**, *141*, 12397−12405.

(72) Yang, S.; Peng, L.; Sun, D.; Asgari, M.; Oveisi, E.; Trukhina, O.; Bulut, S.; Jamali, A.; Queen, W. L. A New Post-Synthetic Polymerization Strategy Makes Metal-Organic Frameworks More Stable. *Chem. Sci.* **2019**, *10*, 4542–4549.

(73) Alkaabi, K.; Wade, C. R.; Dincă, M. Transparent-to-Dark Electrochromic Behavior in Naphthalene-Diimide-Based Mesoporous MOF-74 Analogs. *Chem* **2016**, *1*, 264-272.

(74) Zhao, Q.; Jamal, R.; Zhang, L.; Wang, M.; Abdiryim, T. The Structure and Properties of PEDOT Synthesized by Template-Free Solution Method. *Nanoscale Res. Lett.* **2014**, *9*, 557.

Table of Contents

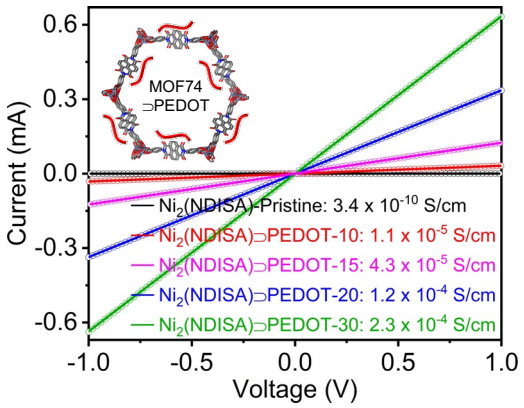

In situ polymerization of PEDOT inside hexagonal pores of an intrinsically collapse-prone, amorphous, and electrically insulating Ni-MOF74 analog yielded robust, crystalline, more porous, and electrically conducting PEDOT@MOF74 composites, as the embedded PEDOT chains at lower concentrations simultaneously reinforced the MOF structure making it more crystalline and porous as well as facilitated charge transport generating electrical conductivity.